University of Bath

Gold interdigitated triple-microelectrodes for label-free prognosticative aptasensing of prostate cancer biomarker in serum

Conlathan Ibau[a], M.K. Md Arshad[a,b,*], Subash C.B. Gopinath[a,c], M. Nuzaihan M.N[a]., M.F.M. Fathil[a], Pedro Estrela[d]

[a]Institute of Nano Electronic Engineering (INEE), Universiti Malaysia Perlis (UniMAP), Kangar, Perlis, Malaysia.
[b]School of Microelectronic Engineering (SoME), Universiti Malaysia Perlis (UniMAP), Pauh, Perlis, Malaysia.
[c]School of Bioprocess Engineering, Universiti Malaysia Perlis (UniMAP), Kangar, Perlis, Malaysia.
[d]Centre for Biosensors, Bioelectronics and Biodevices (C3Bio) and Department of Electronic & Electrical Engineering, University of Bath, Bath BA2 7AY, United Kingdom.

Corresponding author:
Mohd. Khairuddin Md. Arshad (mohd.khairuddin@unimap.edu.my)

Abstract

A simple, single-masked gold interdigitated triple-microelectrodes biosensor is presented by taking the advantage of an effective self-assembled monolayer (SAM) using an amino-silanization technique for the early detection of a prostate cancer's biomarker, the prostate-specific antigen (PSA). Unlike most interdigitated electrode biosensors, biorecognition happens in between the interdigitated electrodes, which enhances the sensitivity and limit of detection of the sensor. Using the Faradaic mode electrochemical impedance spectroscopy (EIS) technique to quantify the PSA antigen, the developed sensing platform demonstrates a logarithmic detection of PSA ranging from 0.5 ng/ml to 5000 ng/ml, an estimated LOD down to 0.51 ng/ml in the serum, and a good sensor's reproducibility. The sensor's detection range covers the clinical threshold value at 4 ng/ml and the crucial diagnosis 'grey zone' of 4-10 ng/ml of PSA in serum for an accurate cancer diagnosis. The selectivity test revealed an excellent discrimination of other competing proteins, with a recorded detection signals at 5 ng/ml PSA as high as 7-fold increase versus the human serum albumin (HSA) and 8-fold increase versus the human glandular kallikrein 2 (hK2). The stability test showed an acceptable stability of the aptasensor recorded at six (6) days before the detection signal started degrading below 10% of the peak detection value. The developed sensing scheme is proven to exhibit a great potential as a portable prostate cancer biosensor, also as a universal platform for bio-molecular sensing with the versatility to implement nanoparticles and other surface chemistry for various applications.

Keywords
 Aptasensor; impedance; interdigitated microelectrodes; prostate-specific antigen; self-assembled monolayer

1.0 Introduction

The proposed sensing strategy is a prognosticative tool to predict the early developmental stage of PCa, which is an alternative to the current detection in practice that rely greatly on the conventional enzyme-linked immunosorbent assay (ELISA) and detects the concentration of prostate-specific antigen (PSA) marker. The high sensitivity and reliability of ELISA are undeniable; however, its requirement for labels, high complexity, labor required, cost and non-portable characteristics have forged the technological loophole that needs to be filled to better suit for the demanding point-of-care (PoC) applications. There is therefore a need for a simpler, cheaper, more reliable, robust and rapid technique to detect cancer biomarkers in blood. Eliminating labels

or tags can lead to a simpler, cheaper alternative to biomarkers detection, however it gives rise to non-specific interactions in complex samples that reduces the device's performance.

One promising technique that warrants the portability, high sensitivity and robustness of surface modification chemistries is the use of screen-printed interdigitated microelectrode. A typical interdigitated microelectrode is made of gold/titanium bilayers on either pristine silica glass or silicon dioxide (SiO_2) substrate. This architecture allows for flexibility to modify the sensing surface either using thiol-gold electrode surface chemistry (Zhurauski et al., 2018)(Arya et al., 2018) or through silanization of hydroxyl (OH) group on the glass/SiO_2 in between the microelectrodes gaps. This modification technique does not only allow for great flexibility in sensor's integration with novel micro- or nano-structured materials, it also allows for highly sensitive electrochemical detection method to be implemented, specifically the electrochemical impedance spectroscopy (EIS)-based sensing. EIS-based detection has gained popularity in biosensing application due to its ability to measure the changes in impedance and capacitance on the electrodes surface upon target binding process across a wide range of target concentration (Wang et al., 2015). With proper equivalent circuit fitting, EIS has the flexibility to be utilized to measure the changes of charge transfer resistance (R_{ct}) using Faradaic mode of detection (in the presence of redox probes), or to measure changes in capacitance, extracted from impedance data using non-Faradaic mode of measurement (without redox probes).

Monoclonal antibody (mAb)-based therapeutics has come a long way in the past four decades since the introduction of the first production technique by Georges Kohler and Cesar Milstein in 1975. As of May 2018, the Food and Drugs Administration (FDA) and the European Medicines Agency (EMA) have approved a total of 80 therapeutic mAb globally (Hongrong Cai, 2018). Despite the inherent features, their main disadvantages include the relatively high production cost, require a longer development time, sensitive to the temperature deviation, and unlike aptamers, the mAbs are only capable of detecting immunogenic targets. Whilst mAbs are the epitome of biomolecular detection, the application of aptamers (aptasensors) has been demonstrated to yield a comparable sensitivity, specificity and affinity to that of mAbs (Gopinath, 2011; Ibau et al., 2017; Savory et al., 2010). Other appealing properties of aptamers over mAbs include smaller sizes (6 – 40 kDa vs. ~150 kDa for mAbs), cost-effective due to high-throughput *in-vitro* selection technology (SELEX) generation technique, and customizable recognition site with a high predilection to the target molecules. Currently, 'Macugen' is the only therapeutic aptamer approved by the FDA for clinical use to treat age-related macular degeneration (AMD) of the retina, however several others are in approval stage (Stein and Castanotto, 2017). Unlike the antibodies which rely on the immunogenic response, aptamers hold the unprecedented potential for a greater flexibility to 'sense' for a wider range of target molecules (Bagheri et al., 2018; Feng et al., 2014; Seok Kim et al., 2016).

We here report the findings on the development of highly sensitive and specific gold interdigitated triple microelectrodes-based sensor to detect PSA using an anti-PSA aptamer. The in-house fabricated sensing microelectrodes were chemically modified through amino-silanization on the SiO_2 gap between the patterned gold triple microelectrodes. This technique allows for sensitive detection and estimation of different concentrations of PSA antigen by measuring the changing surface resistance on the device, which translates to the changes in R_{ct} and total impedance of the EIS measurement system. The use of interdigitated microelectrode enables for a greater flexibility in the sensing surface modifications and the use of robust, highly sensitive PSA target detection schemes, e.g. measurement in (i) the changes of surface resistance and (ii) the capacitive effects in the EIS setup. The microelectrode arrays increase the effective sensing area that enables for greater DNA-aptamer probe loading and PSA binding event. Further increase in the effective sensing surface area-to-volume ratio is achievable through the

deposition of nanoparticles and novel nanostructured materials, i.e. molybdenum disulfide (Dalila R et al., 2019) in between the microelectrode gaps. Moreover, the authors demonstrate the device architecture does not only exhibit an exceptional detection performance, but also to benefit from the inherent portability feature and the high-volume fabrication capability of the device.

2.0 Experimental

2.1 Materials and reagents

A 32-nucleotide carboxyl-terminated anti-PSA DNA aptamer (5'-COOH-C_6-TTT TTA ATT AAA GCT CGC CAT CAA ATA GCT TT-'3) was procured from Integrated DNA Technologies (IDT, Singapore). The sequence was modified from the work reported in (Savory et al., 2010), in which a genetic algorithm (GA) was applied to post-SELEX screening of the oligonucleotide, and resulted in 48-fold higher binding affinity compared to those obtained from SELEX alone, and a dissociation constant (K_D) in tens of nM. Prostate-specific antigen (PSA) was procured from Fitzgerald (MA, USA), and diluted into different testing concentrations in Buffer A, which consists of 100 mM PBS (pH 7.4). 3-Aminopropyltrimethoxysilane (APTES), 1-ethyl-3-dimethylaminopropylcarbodiimide hydrochloride (EDC), N-hydroxysuccinimide (NHS), potassium buffer saline tablets (pH 7.4), potassium hexacyanoferrate (III), and potassium hexacyanoferrate (II) were all purchased from Sigma Aldrich (Malaysia). StartingBlock phosphate buffer saline-Tween 20 (SBPBS-T20), as termed Blocker A in this report was procured from Fisher Scientific (UK). All other reagents were of analytical grade, and all aqueous solutions were prepared using 18.2 MΩ ultra-pure Milli-Q water, and further filtered through Pyrogard® 0.22 μm pore filter (Millipore, MA, USA).

2.2 Measurement and apparatus

The morphology of the sensing surface was characterized via atomic force microscopy (AFM) in ambient tapping mode using SPA400-SPI4000 AFM (Seiko Instruments Inc., Japan) in conjunction with Nano Navi SPA400 software for imaging and analyses. The morphological profiles were imaged using 10 nm in diameter SI-DF20 cantilever (Seiko Instruments Inc., Japan), at spring constant of 11 N/m and resonance frequency of 122 kHz. The water contact angle was measured using an in-house built optical angle measurement system (Miodek et al., 2015). The measurement was carried out by dispensing 30 μl of water droplet onto the electrode surface, and subsequently, Nikon COOLPIX P520 camera with 18.1 megapixels sensor was used to capture the contact angles at a fixed focal length of 37 mm. OnScreenProtractor version 0.5 (Iconico) was used to measure the contact angle.

An X-ray photoelectron spectroscopy (XPS) model XPS XSAM-HS (Kratos, UK) with focused monochromatic Mg Kα X-ray source (run at 120 W) was used to characterize the surface elemental analysis to validate sensing surface functionalization. The chamber pressure was set at 5 x 10^{-8} torr for each sample analysis, in which was recorded in the energy range between 10 to 1100 eV, where the pass energy and step size were set at 150 and 1 eV per step. The peak analysis was performed using CasaXPS processing software version 2.3.16, and references for peaks analysis were made from the XPS handbook and the National Institute of Standard and Technology (NIST) XPS online database. Electrochemically, the sensors were characterized in Faradaic mode of detection using a μAUTOLAB III/FRA2 potentiostat (Metrohm Autolab, Netherlands). Validation of successful sensing surface functionalization and probe binding was carried out via cyclic voltammetry (CV) in a three-electrode configuration as reported in (Arya et

al., 2018). CV measurement was performed in Buffer B, which consists of 50 µl of 100 mM PBS (pH 7.4) containing 2 mM $[Fe(CN)_6]^{3-/4-}$ redox couple at scanning potential of -0.6 V to 0.6 V. Detection and estimation of binding event at different concentration of PSA onto aptamer were done via Faradaic mode EIS. The impedance spectrum was measured using gold as counter (2 mm width) and pseudo-reference electrodes at an open circuit potential (OCP) in the frequency range of 100 kHz to 0.5 Hz, with a 100 mV amplitude in Buffer C, consists of 50µl of 100 mM phosphate buffered saline (PBS) buffer (pH 7.4) containing 5 mM $[Fe(CN)_6]^{4-}$ (ferrocyanide) and 5 mM $[Fe(CN)_6]^{3-}$ (ferricyanide) redox couple on the sensing surface.

2.3 Microelectrode preparation and functionalization

2.3.1 Fabrication of gold interdigitated electrodes

The interdigitated electrodes were fabricated using a conventional micro-fabrication technique, with a simple, single-masked photolithography process for structural patterning and development of the device. Briefly, a bilayer negative photoresist (NR7-3000PY/NR71-3000P Futurrex, USA) was spin-coated onto the silicon/silicon dioxide substrate and the chrome mask with interdigital fingers of 10 µm in width and 3500 µm in length, with spacing in between fingers at 10 µm that spread over 6000 µm was transferred onto the resists. Subsequently, Ti/Au bilayers (~20 nm/~250 nm) were evaporated successively onto the developed photoresists, and then the bi-layer photoresists were 'lifted-off', leaving behind the patterned gold interdigitated electrodes on the substrate.

2.3.2 Sensing surface modifications

Prior to surface functionalization procedures, a batch of three gold interdigitated electrodes were cleaned thoroughly by sonication in acetone, isopropanol (IPA), and Milli-Q water, followed by nitrogen blow dry, and then 30 min of ultraviolet (UV)-ozone treatment in ProCleaner (Bio-Force Nanoscience, USA). A self-assembled monolayer (SAM) layer was obtained through amino-silanization of the hydroxyl group onto the SiO_2 gap in between gold interdigitated as reported in (Zhu et al., 2012) with slight modifications. Briefly, the cleaned devices were immediately placed in a desiccator, followed by incubation with 50 µl of 2% APTES (pre-diluted to working concentration in anhydrous toluene) for 120 min at 70°C. The unreacted APTES was then rinsed with toluene (2x), absolute ethanol (2x), and Milli-Q water (2x), and followed by drying in a muffle furnace at 110°C for 15 min. The silanized devices were hydrolytically stabilized overnight in Milli-Q water at 40°C, subsequently rinsed with Milli-Q water and dried in a muffle furnace at 110°C for 15 min. Before use, the carboxyl-terminated anti-PSA DNA aptamer was first heated to 90°C for 2 min to unfold its structure and cooled down to room temperature (RT). Next, 990 µl of 2 µM DNA aptamer, diluted to working concentration in Buffer A was incubated into the mixed solution (1:1 v/v) of 10 µl 400 mM EDC/100 mM NHS cross-linker for 30 min to activate the carboxyl group on the aptamer. Then, 50 µl of 2 µM EDC-activated DNA aptamer was incubated onto the APTES-functionalized electrodes for 60 min to allow for DNA aptamer binding on the SAM surface. To avoid deposition of the negatively charged DNA aptamer onto the gold electrodes through electrostatic interaction which may lead to high background noise during measurements, the electrode was biased with a

small potential of -75 mV to repel the aptamer from the gold electrode. Thereafter, the unreacted DNA aptamer was rinsed with a copious amount of Buffer A, and subsequently, the unbound active sites were blocked using undiluted Blocker A for 15 min, then rinsed off the extra solution on the electrodes surface. Otherwise mentioned, all the steps were performed at RT. The functionalized interdigitated electrodes were stored in 4°C fridge until further use. Fig. 1 shows the overall process for micro-fabrication and surface modification on the transducer surface of the interdigitated microelectrodes.
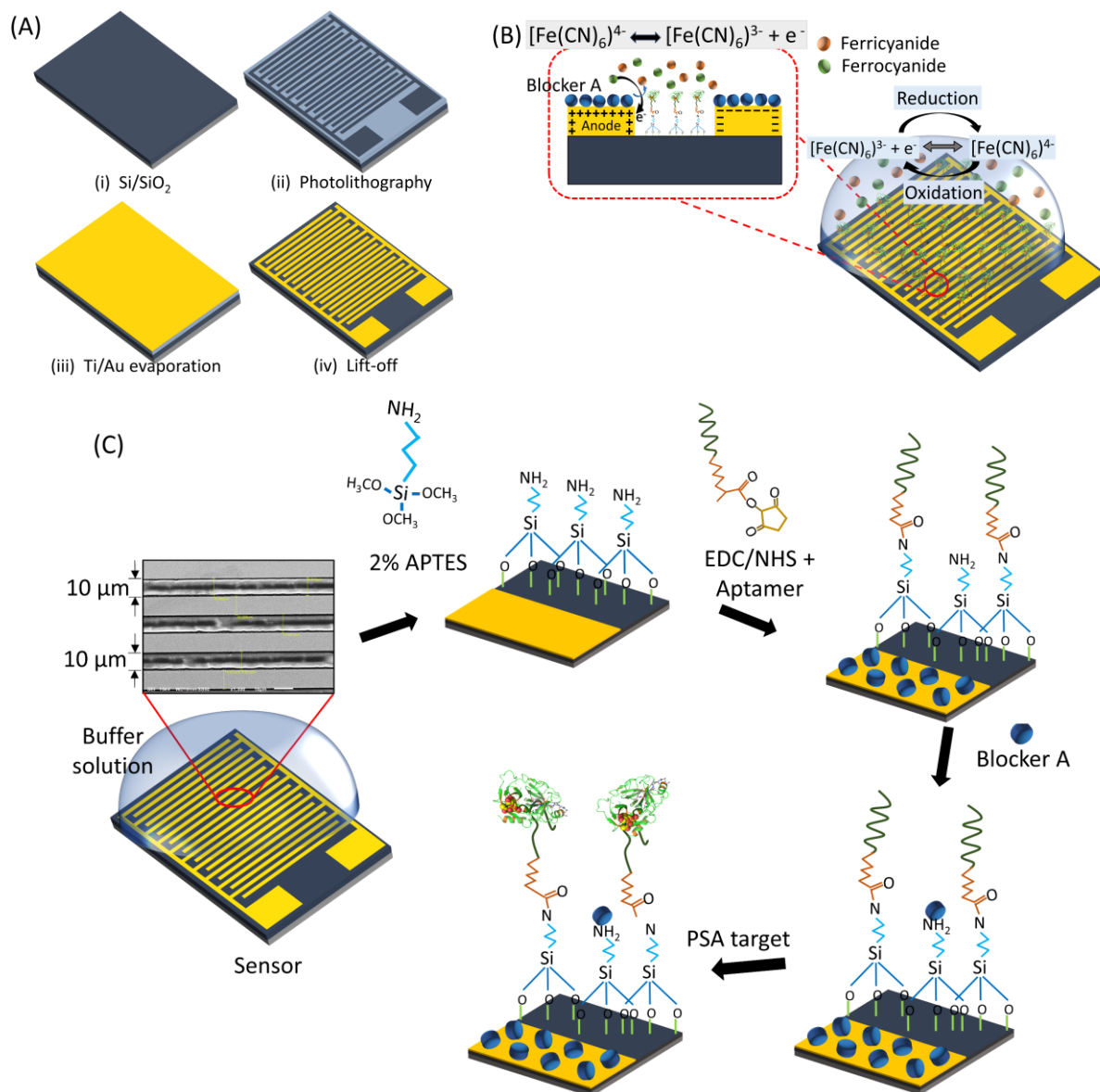

Fig. 1A(i-iv). The conventional photolithography process steps to fabricate the gold interdigitated microelectrode. Fig. 1B. The Faradaic EIS detection scheme for PSA target on sensing surface. Fig. 1C. Representation of surface modification techniques on the electrode surface for the detection of PSA protein. Images drawn not according to the actual dimensions.

3.0 Results and discussion

3.1 X-ray photoelectron spectroscopy (XPS) characterization on sensing surface

XPS technique was used to quantify the elemental composition and chemical state on the functionalized sensing surface (scan depth ~5-10 nm), thus validated the presence of the desired functional groups that are responsible for the binding of targeted linking chemistries. All spectra peaks were calibrated according to the inherent 'adventitious' carbon, C 1s peak at a binding energy (BE) of 284.8 eV due to the air-exposed samples which correspond to the presence of C-C hydrocarbon bonds. The XPS survey spectra for the sensing electrode's modification steps are shown in Fig. 2A(i).

Fig. 2B(i) shows the Si 2p narrow spectra which revealed three distinct peaks at BE of 99.8 eV showing the presence of SiO_2 on the pristine electrode surface. Upon treatment using APTES, the presence of peaks at 101.7 eV and 102.2 eV validate the formation of silane (SiH_4) group through the silanization of APTES with the hydroxyl group on the SiO_2. These two distinct peaks are corresponding to the type of amino-silane formation on the pristine substrate, i.e. single monolayer at 101.7 eV and multilayer formation at 102.2 eV. These self-assembled layers were formed when the reactive methoxy (OCH_3) head groups of APTES was hydrolyzed to silanol (Si-OH), subsequently tethered the silane molecules onto SiO_2 through condensation process (Dietrich et al., 2016), as shown in Fig. 2A(ii). The C 1s spectra shown in Figure 2B(ii) validate all the functional groups present in APTES functionalized surface with good agreement with works reported in (Cao et al., 2009; Evans, 1997), i.e. alkyl carbon, C-C (284.8 eV), carbon atoms with single bond to oxygen or nitrogen, C-N/C-O (286.3 eV) and an amide, O=C-N (288.1 eV). Though, these peaks could be resulted from the inherent hydrocarbon contamination due to the air-exposed samples (Acres et al., 2012), the significant increment in the peak intensity before and after APTES modification step further validate the presence of functional moieties from APTES functionalization. The increment in O=C-N (amide) peak at 288.1 eV with post-aptamer immobilization step confirmed the successful binding of EDC-activated anti-PSA aptamer onto the silanized SiO_2 surface. Another validation on successful aptamer immobilization was shown in Fig. 2B(iv), showing two distinct P 2p peaks at 132.5 eV and 133.6 eV that confirm the presence of the conjugated DNA aptamer's sugar-phosphate backbone on the sensing surface (Chung et al., 2018; Wang et al., 2018). Fig. 2B(iii) shows the N 1s peaks at BE of 400.1 eV and 401.9 eV further validated the presence of unbounded free amine (NH_2) group and hydrogen-bound amine (H-NH_2) group, the characteristics of successful surface functionalized with APTES (Acres et al., 2012; Vandenberg et al., 1991).
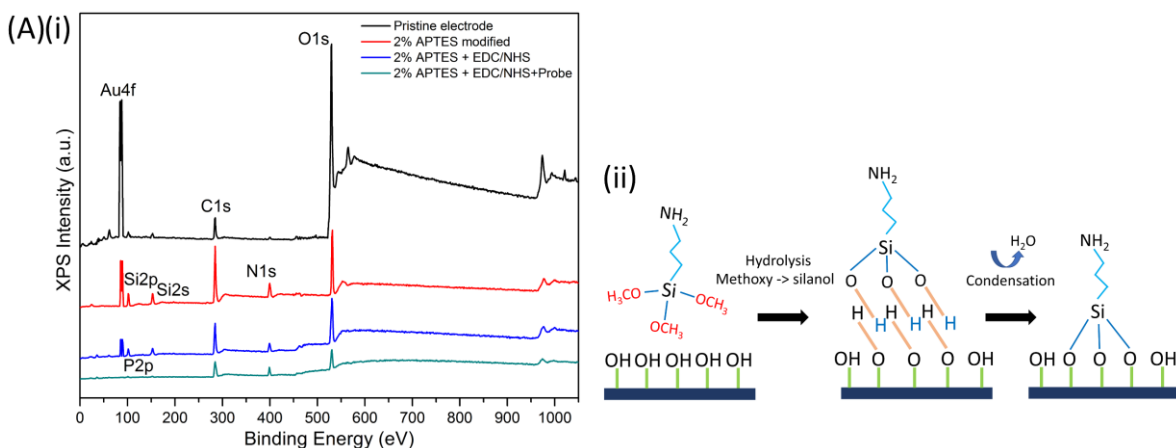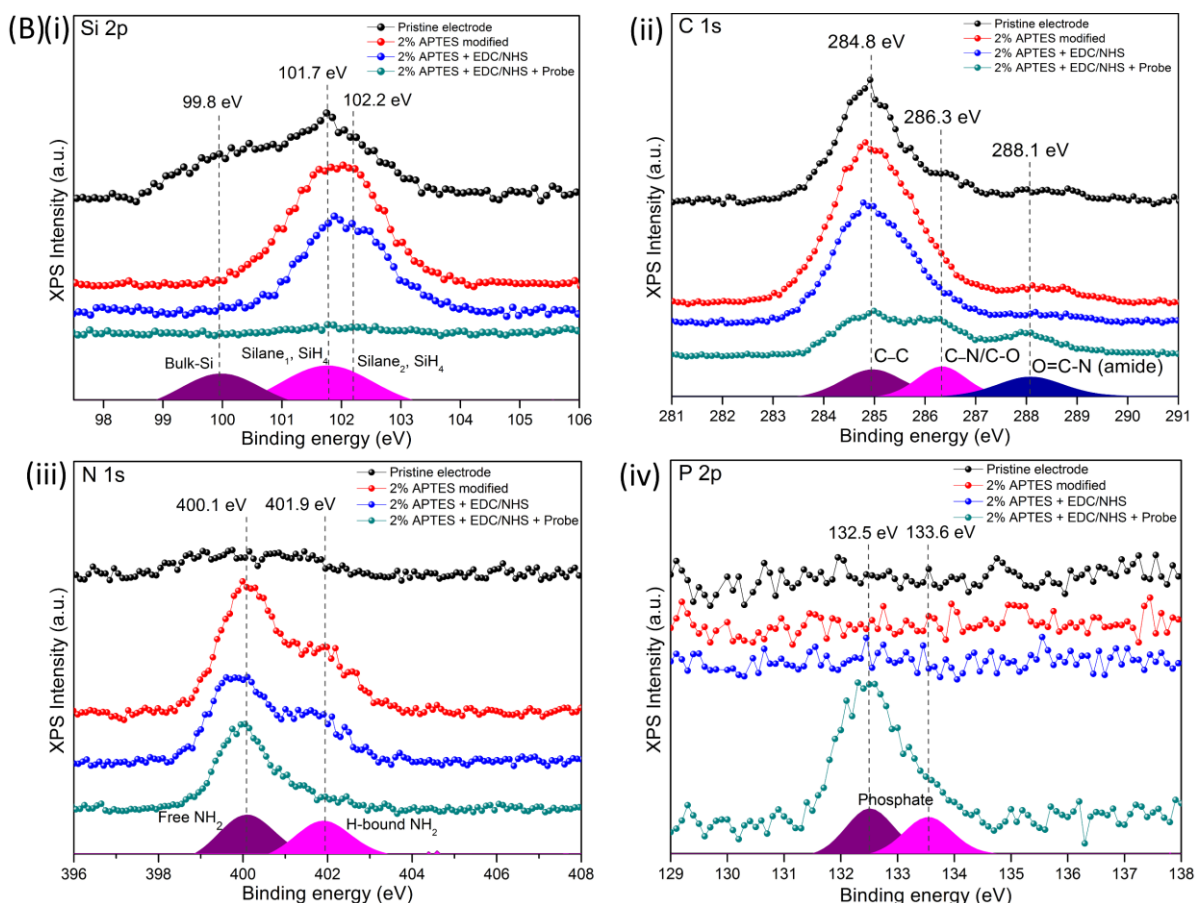
Fig. 2. XPS spectra analysis of surface functionalization on the sensing surface. Fig. 2A(i). An overlay of XPS survey spectra for each electrode modification step. Fig. 2A(ii). APTES silanization process with a hydroxyl group on SiO$_2$ substrate. Fig. 2B(i-iv). High-resolution narrow peaks of Si 2p, C 1s, N 1s and P 2p with respect to the binding energy (BE).

3.2 Cyclic voltammetry (CV), atomic force microscopy (AFM) morphology and hydrophobicity study via water contact angle measurement

Besides XPS quantification, CV scan was performed in Buffer B to further validate the aptamer-probe immobilization on the sensing surface. The changes in the working electrode, WE peak current (µA) over the range of cycling potential at -0.6 V to 0.6 V were recorded, as shown in Fig. 3A. Prior to any modifications, the pristine electrode shown in Fig. 3A(i) recorded a low surface resistivity with peak current at 305.3 µA, which shows a clean, conductive electrode. In Fig. 3A(ii), the modification with APTES has drastically reduced the peak current from 305.3 µA to 211.4 µA due to an increase in surface resistance due to the successful formation of the SAM layer in between the interdigitated gaps due to the APTES silanization. The peak current was further reduced to 168.7 µA upon immobilization with EDC-activated anti-PSA aptamer probe, as shown in Fig. 3A(iii). Furthermore, after the sensing surface was blocked with Blocker A protein, the peak current was further reduced to 155.3 µA. This reduction confirms the full coverage of the free surface by the blocking proteins.

Fig. 3B shows the morphological study on the modified electrode's surface, (i) APTES – EDC/NHS coupling, and (ii) anti-PSA aptamer bound surface using AFM characterization in tapping mode. The images showed drastic changes in the overall surface roughness

after the aptamer immobilization. The mean surface roughness (R_a) and maximum roughness (R_{max}) had decreased from 1.23, 9.37 down to 0.98, 5.66 respectively, which suggested successful binding of the aptamer on the electrode's surface. Furthermore, water contact angle measurements were conducted to further validate the binding of the aptamer. As shown in Fig. 3C(i), the promotion of OH functional group after the UV-ozone treatment has rendered the sensing surface hydrophilic. Besides promoting the OH for silane tethering, UV-ozone treatment is an effective electrode's cleaning technique after the sonication in acetone, IPA and Milli-Q water. APTES silanization on the substrate introduced alkyl chains and amino groups, an evident in the increased in water contact angle from hydrophilic surface to 73.32 ± 2° as shown in Fig. 3C(ii), which is comparable to the finding reported in (Cao et al., 2009). In Fig. 3C(iii), upon DNA aptamer binding event the contact angle was further reduced to 61.45 ± 2°, confirming the successful binding of anti-PSA aptamer onto the sensing surface.
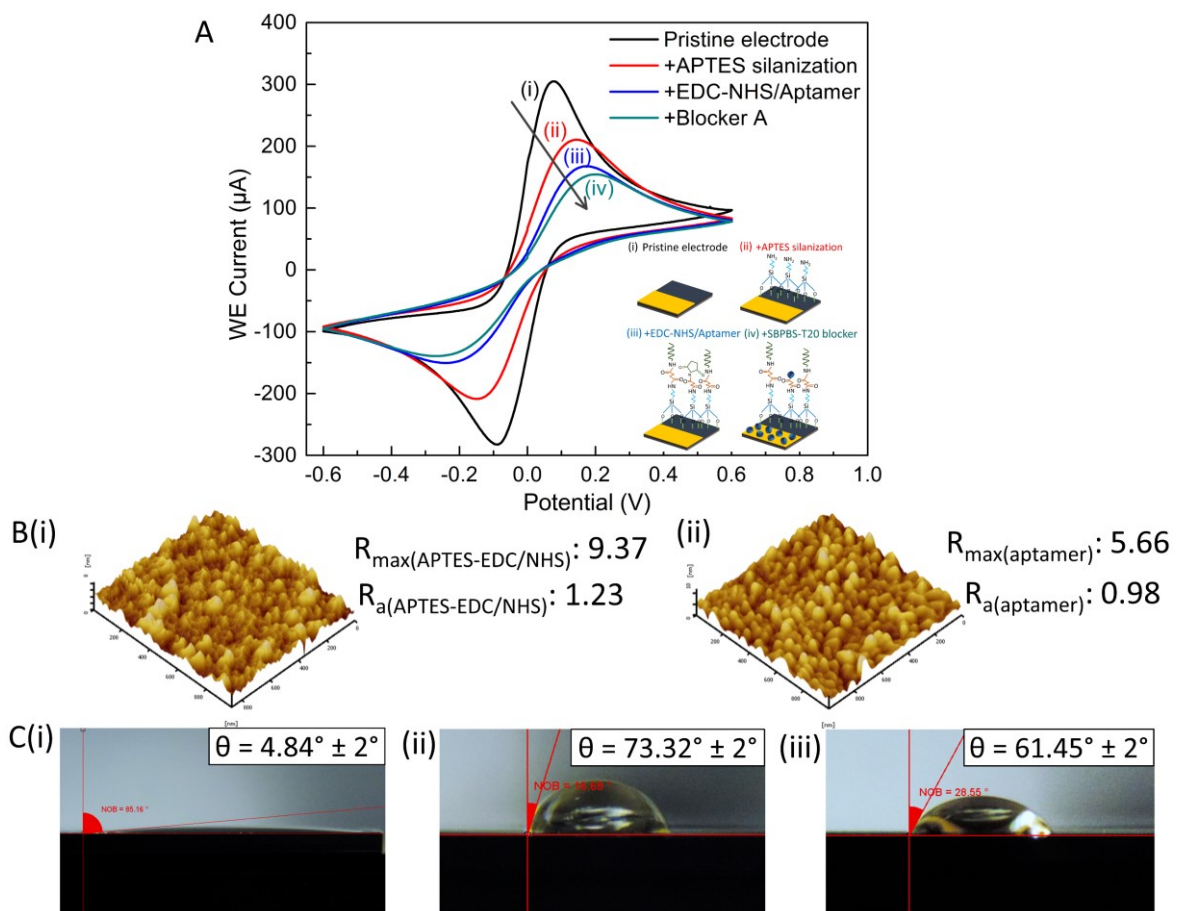

Fig. 3. Electrical and optical characterizations of the sensing surface's functionalization process using (A) CV measurement in Buffer B, (B) atomic force microscopy (AFM) characterization, and (C) water contact angle measurement techniques.

3.3 Quantification of PSA detection via impedimetric measurement in Faradaic EIS mode

The interaction between immobilized anti-PSA aptamer against different concentrations of PSA was carried out by incubating 50 µl of the diluted antigen (pre-diluted to working concentration in Buffer A) onto the sensing surface in a batch of three devices for 60 min at 37°C. The devices were then rinsed with a copious amount of Buffer A, subsequently, incubated in 50 µl of Buffer C for 10 min to stabilize the SAM layer. The

impedance spectrum was then measured in 50 μl Buffer C at an open circuit potential (OCP) in the frequency range of 100 kHz to 0.5 Hz, with a 100 mV amplitude perturbation.

The detection scheme was carried out by measuring the changes in the charge transfer resistance, R_{ct} (represented by Nyquist plot) and the total impedance, Z versus frequency (represented by Bode plot) of the electrochemical system due to the PSA – aptamer binding onto the modified interfacial layer, i.e. the microelectrode gaps that caused the disruption to the equilibrium potential of the $[Fe(CN)_6]^{4-/3-}$ redox couple. In this measurement, the change in the R_{ct} values correspond to the alteration of the modified interfacial layer on the microelectrode gaps causing the changes in the intensity of electrons transfer from the redox species onto the microelectrode surface as depicted in Fig. 1B, in which the magnitude of the changes is according to the concentration of PSA bound onto the aptamer (Park et al., 2018). Moreover, the gold microelectrode surface was effectively blocked using the Blocker A (refer to Fig. 1B). Besides avoiding the non-specific binding, the step ensures a consistent charge transfer between the redox potential and the gold electrode surface, hence any modification onto the interfacial layer, such as the biomolecular binding event would result in a very specific, highly sensitive change in the magnitude of R_{ct} values. Moreover, the modification of the interfacial layer was performed in between the microelectrode's gaps which enhances the device's sensitivity in detecting slight changes in the resistance of the charge transfer in the redox potential due to the target molecule's binding.

Two types of detection data were reported in the findings, firstly the Nyquist plot as shown in Fig. 5A(i) and Bode plot in Fig. 5A(ii). The Nyquist plot shows the -Z" vs. Z' relationship upon interaction with different PSA concentrations from 0.5 ng/ml down to 5000 ng/ml. Prior to the sensor's surface modification, the pristine electrode surface exhibits the lowest R_{ct} value of 153 Ω due to the absence of the resistive APTES SAM layer on the electrode, as shown in the inset (b) of Fig. 5A(i). The successful SAM assembly, aptamer immobilization and Blocker A blocking protein resulted in a drastic increased in ΔR_{ct} recorded at 5.804 kΩ (mean R_{ct} value measured across a batch of three sensors, n=3). The successful binding of PSA target is validated via the reduction of R_{ct} values which took place in the presence of PSA antigen, and these changes occurred only at the R_{ct} value above that of the 'Aptasensor' baseline value. Inset (a) of Fig. 5A(i) shows the schematic diagram of the equivalent Randles circuit used for electrochemical fitting, where R_s is the resistance of electrolyte solution, Q is a constant phase element (CPE) and Z_w is Warburg impedance. The Bode plot in Fig. 5A(ii) exhibits a similar trend as the Nyquist's for different concentrations of PSA. This is due to the higher density of bound PSA molecules onto the aptamer increases the total Z values on the sensing surface. The sensors responded to these changing effects at a frequency below 10^4 Hz, as evident from the increasing impedance values against the decreasing frequency. The magnitude of slope from the impedance curve directly corresponds to the abundance of ions or molecules adsorbed on the sensing surface (Madianos et al., 2018), i.e. the binding of PSA molecules on the aptamers. For the frequency range above 10^4 Hz, the constant impedance value (the horizontal line from frequency 10^4 to 10^5 Hz) represents the measured fixed value of R_s, irrespective to the modification on the sensing surface or molecular binding event.

The linearity response for the increase of R_{ct} and total Z against the increasing PSA concentrations are depicted in Fig. 5B(i) and Fig. 5B(ii), respectively. Fig. 5B(i) shows the calibration curve with respect to the Nyquist response, plotted from mean changes in R_{ct} (kΩ) from the 'Aptasensor' baseline values (without the introduction of PSA) at 2.0 Hz versus the logarithmic scale of PSA concentration in PBS (ng/ml). The calibration curve

shows the capability of the sensors for a linear detection of PSA antigen in the range of 0.5 ng/ml down to 5000 ng/ml, following the linear equation ΔR_{ct} (kΩ) = 0.659 [kΩ] + 0.673 $\log_{10}$ [PSA] (ng/ml). The sensors exhibit a sensitivity of 0.673 kΩ/$\log_{10}$ ([PSA] ng/ml) and a correlation coefficient (R^2) of 0.978. The limit of detection (LOD) and limit of quantification (LOQ) were estimated as 0.413 ng/ml and 10.078 ng/ml, respectively, using the linear regression analyses (Shrivastava and Gupta, 2011). The estimation of LOD and LOQ were expressed using the formulae:

$$LOD = \frac{3\alpha}{b},$$
$$LOQ = \frac{10\alpha}{b},$$

where α is the standard deviation of the sensor's response, estimated from y-residuals of the calibration curve and b is the sensitivity of the sensors computed from the slope of the calibration curve. Meanwhile Fig. 5B(ii) shows the calibration curve with respect to the Bode response, plotted from the mean changes in total Z values (kΩ) from the baseline values at 2.0 Hz versus the logarithmic scale of PSA concentration in PBS (ng/ml). This Bode response-based calibration curve reveals a linear detection in the range of 0.5 ng/ml to 5000 ng/ml following a linear equation ΔZ (kΩ) = 2.139 [kΩ] + 2.710 $\log_{10}$ [PSA] (ng/ml), a sensitivity of 2.710 kΩ/$\log_{10}$ ([PSA] ng/ml), and R^2 of 0.993. Interestingly, the response shows a slightly lower LOD and LOQ, estimated at 0.377 ng/ml and 2.686 ng/ml respectively. This reduction in the estimation of LOD and LOQ is due to greater linearity response from the Bode data, hence resulting in a higher confidence level in estimating both limits.

Table 1 shows the comparison in sensing performance of the reported work to other assays. It is shown that the developed sensor exhibits a comparable linear detection range to other reported assays. In this work, the authors demonstrated the use of a simpler and cost-effective approach to obtain a linear and acceptable detection limit without the use of graphene derivative materials which bare extra development cost. The reported approach is applicable for the application of prostate cancer's detection which has a clinical cut-off value of 4 ng/ml.
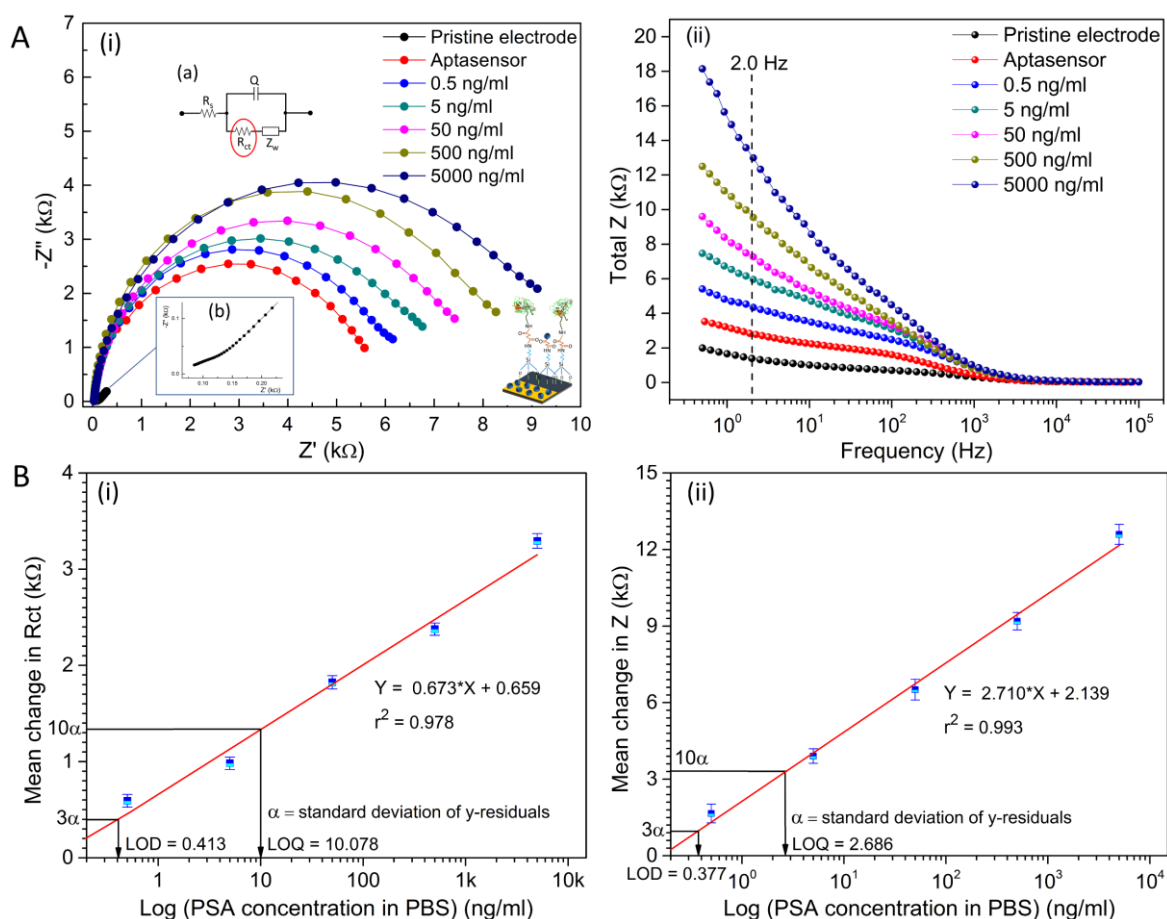
Fig. 5. EIS responses of developed sensing devices to detect different concentrations of PSA antigen, measured in Buffer C. A(i). The -Z" vs. Z' 'Nyquist plot' with an inset (a) showing the equivalent Randle's circuit. A(ii). The total Z vs. frequency 'Bode plot'. Fig. B. The calibration curve with respect to (i) Nyquist plot and (ii) Bode plot.

3.4 Demonstration of PSA estimation in physiological serum

The feasibility of the developed sensors for clinical applications was tested in undiluted human serum spiked with concentrations of PSA ranging from 0.5 ng/ml to 5000 ng/ml. The setup evaluates the ability for the sensors to detect the PSA molecule, while discriminating other inherent proteins in the serum, demonstrating high specificity of the sensors. The Faradaic mode EIS technique was implemented to detect PSA in the serum, meanwhile with Bode plots used to illustrate the detection results due to its greater linearity as demonstrated for detecting PSA in PBS solution. Fig. 6 shows the PSA sensing performance in undiluted serum. Prior to detecting the diluted range of PSA, the assay was first subjected for the dose-response test with concentrated 1 µg/ml of PSA to first evaluate as if the sensors respond to the concentrated dose of the analyte.

Fig. 6(i) shows the dose-response before and after the introduction of the target antigen. At 2.0 Hz, the sensors demonstrated the highest percentage increase in total Z (kΩ) by 237.82% and -phase (°) change by 143.99% after the binding event. Hence, subsequent analyses were carried out at the sensor's highest response at 2.0 Hz. Fig. 6(ii) depicts the Bode plot for the detection of PSA in undiluted serum. The sensors exhibit a similar response towards the different concentrations of PSA as compared to the identical assay in PBS. However, a reduction in the overall magnitude of total Z (kΩ) was observed for detecting each of PSA dilutions. This could be due to the increase in the total

Z of the electrolyte due to the presence of other proteins in the undiluted human serum. However, the sensors were able to distinguish in sensing PSA antigen from other proteins as evident from an increasing trend in total Z values against the increasing concentration of PSA in the serum. Similar to the assay in PBS, this detection assay's response to changes in PSA concentrations within the frequency range $<10^4$ Hz.

The calibration curve in Fig. 6(iii) validates a linear detection of PSA in the undiluted human serum with a linear range of 0.5 ng/ml down to 5000 ng/ml following a linear equation ΔZ (kΩ) = 0.907 [kΩ] + 1.212 $\log_{10}$ [PSA] (ng/ml), a sensitivity of 1.212 kΩ/$\log_{10}$ ([PSA] ng/ml), and R^2 of 0.989. As compared to the assay tested in PBS, in undiluted serum, it was observed that both estimated LOD and LOQ have increased to 0.510 ng/ml and 5.903 ng/ml respectively. These increases in LOD, LOQ and lower sensitivity of detection at 1.212 kΩ/$\log_{10}$ [PSA](ng/ml) in serum as compared to PBS were caused by the greater background noise due to higher abundance of competing proteins against the aptamer in the serum. Nonetheless, the sensors demonstrate a great degree in discriminating the non-specific proteins in the serum, hence proving the applicability of the developed sensors as a feasible approach for estimating the abundance of PSA antigens in clinical settings.
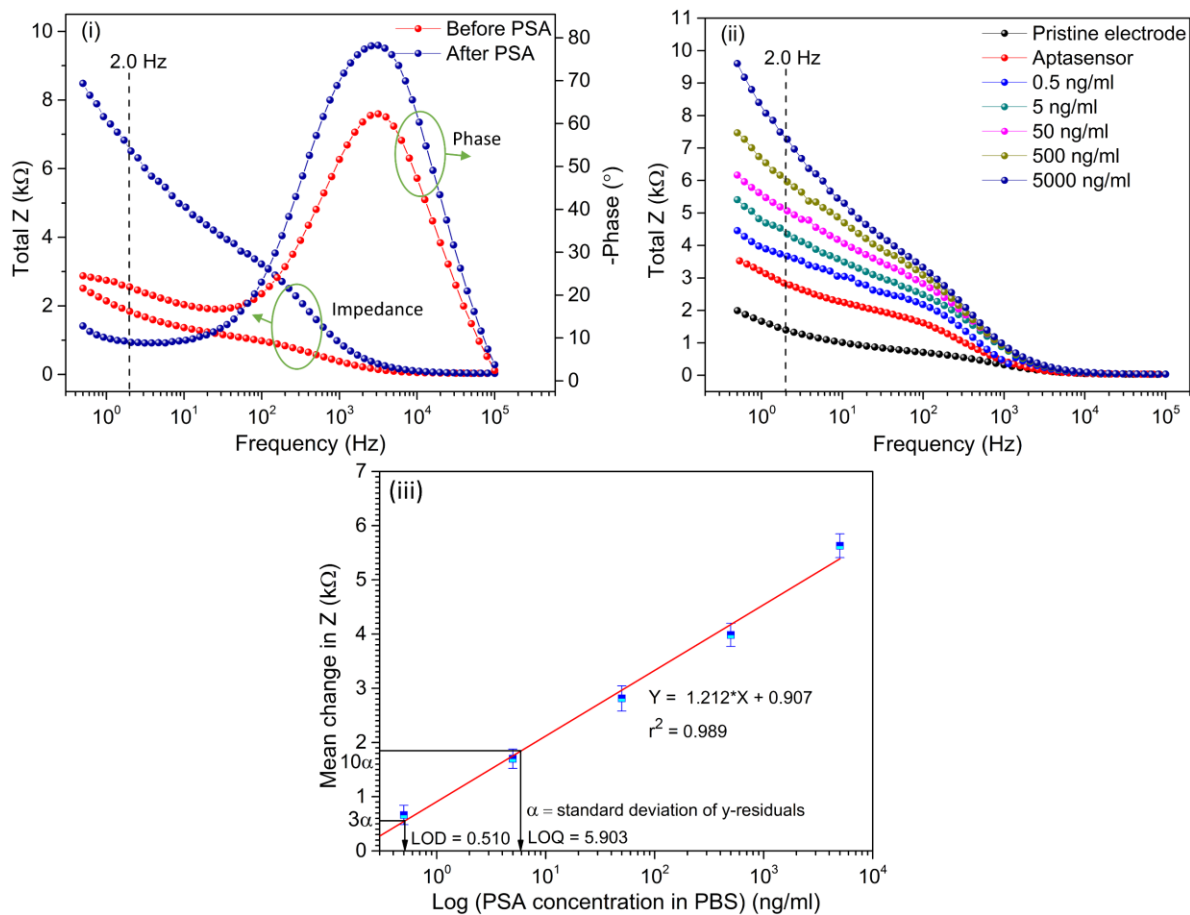

Fig.6. The feasibility study of EIS responses for evaluating sensor's specificity, tested against different concentrations of PSA in undiluted human serum. (i). Dose-response for changes in total Z and phase data versus frequency before and after PSA binding at 1 µg/ml. (ii). Bode plot for detection of different concentrations of PSA. (iii). Calibration curve showing linear detection of PSA concentration in undiluted human serum.

3.5 Reproducibility, selectivity and stability studies of the developed sensor

The sensing performance of the developed sensing architecture was tested to validate the reliability of the detection results. Fig. 7(i) shows the bar graph with SD error bars of a batch of three tested sensors, with relative standard deviation (R.S.D) for n=3 in detecting each diluted PSA concentrations of 0.5 ng/ml – 5000 ng/ml. The data show a good reproducibility with highest R.S.D of 4.24% (n=3). Another test was conducted to study the selectivity of the sensors in sensing PSA versus human serum albumin (HSA) and human glandular kallikrein 2 (hK2) as negative control, tested at selected concentrations of 5 ng/ml and 50 ng/ml. hK2 is another prostate-specific kallikrein marker which has 80% DNA sequence homology to PSA. Successful discrimination in detecting PSA target against hK2 therefore demonstrate a high selectivity performance of the sensor. Fig. 7(ii) shows an excellent selectivity with a recorded detection of PSA signal of 9-fold increased versus HSA and 6-fold increased versus hK2 at tested concentration of 5 ng/ml. At 50 ng/ml, the PSA detection signal recorded a 7-fold increase versus HSA and 8-fold increase versus hK2, which demonstrate an excellent selectivity of the device. Fig. 7(iii) shows the stability study for the sensor for each of the surface modification step. The inset figure depicts the measured relative Z values degradation of the Aptasensor bound to the 5 ng/ml PSA target, in which the Aptasensor were stored for 3 weeks and a batch of sensors (n=3) were tested for binding stability with PSA target at every three consecutive days. The aptasensors were stored in 100 mM PBS solution (pH 7.4) at RT throughout the duration. In this study, the measured Z values which had degraded more than 10% of the peak signal were considered losing its stability. From the figure, the aptasensor retained its stability for six (6) days before the Z values plummeted below 10% from the peak value. This degradation in Z value could be hypothesized due to the DNA aptamer folding event and the protein denaturation tested at RT which altered the electrical characteristics on the sensing surface over the prolonged tested duration. Another probable contributing factor is the unavailability of strong carboxyl (COOH)-modified aptamer 5' end due to the nature of the aptamer secondary structure. This limitation may hinder the prolonged aptamer attachment after the tested 6 days period. Due to the same reason, the APTES modified surface may not hold the aptamer after the stated stability period of 6 days.
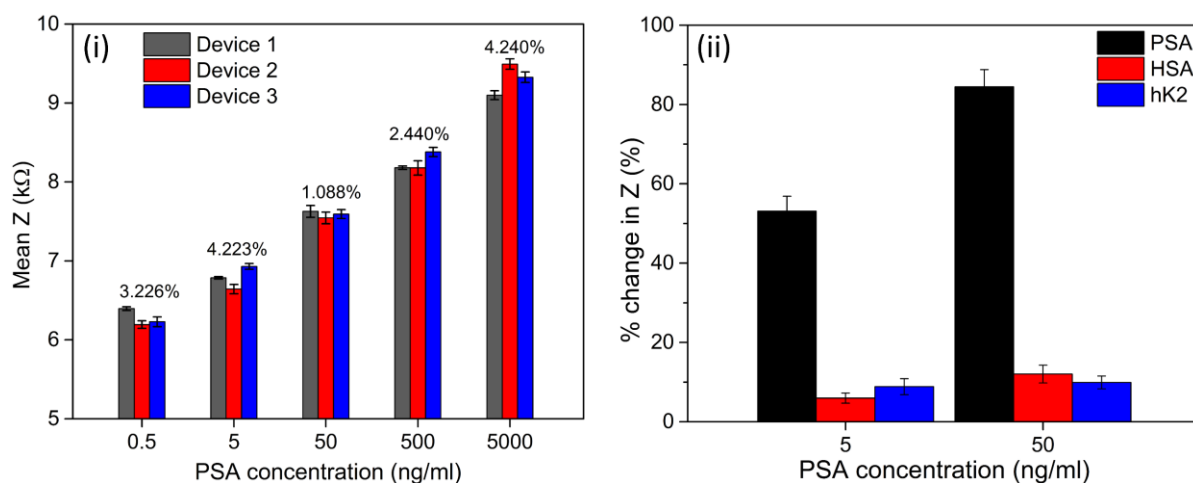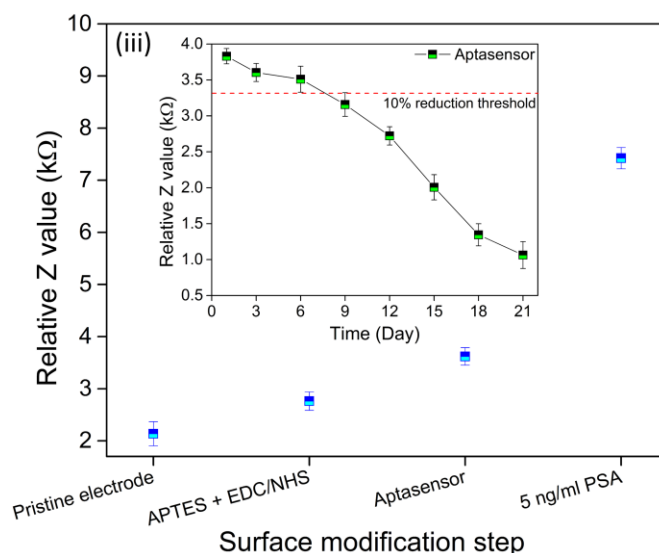
Fig. 7. Sensor's performances. (i). Reproducibility data of the detection assay with calculated R.S.D for n=3. (ii). Selectivity data for the sensors in discriminating undiluted HSA against PSA and hK2. (iii). Stability performance of the sensor.

Table 1

Performance comparison of the developed sensor

Scheme	Assay	Probe immob. strategy	Sample volume	Detection range	LOD	Ref.
GCE	CV/EIS	GCE/SP-rGO-GA/anti-PSA mAb	N/A	80 ng/ml − 0.1 ng/ml	53.00 pg/ml	(Wang et al., 2015)
GCE	DPV/EIS	GCE/rGO-chitosan/GA/TH-anti-PSA mAb-TH	10 μl	90 ng/ml − 0.1 pg/ml	10.00 fg/ml	(Kavosi et al., 2015)
GCE	Ampero	GCE/GO-PDDA-chitosan/peptide-IL	80 μl	100 ng/ml − 1 fg/ml	1.00 fg/ml	(Tang et al., 2017)
IDE	EIS	Cr-Au/Cys-SAM/EDC-NHS/anti-PSA mAb	N/A	100 ng/ml − 1 pg/ml	1.00 pg/ml	(Arya and Bhansali, 2012)
Au disc	CV/EIS	Au/L-cysteine-SAM/EDC-NHS/anti-PSA mAb	N/A	30 ng/ml − 1 ng/ml	0.03 ng/ml	(Spain et al., 2016)
Carbon SPE	Ampero /CV	SPE/MPs-anti-PSA scAb	N/A	10 ng/ml − 1 ng/ml	0.50 ng/ml	(Zapatero-Rodríguez et al., 2018)
Au IDE	CV/EIS	IDE/APTES/EDC-NHS/anti-PSA aptamer	50 μl	5000 ng/ml − 0.5 ng/ml	0.51 ng/ml (in serum)	*This work*

Note: GCE: Glassy Carbon Electrode, IDE: Interdigitated electrode, MGIDEA: Micro-gapped Interdigitated Electrode Array, SPE: Screen-printed Electrode, SP: silk peptide, rGO: reduced graphene oxide, GA: glutaraldehyde, TH: thionine, PDDA: Poly (dimethyldiallyammonium chloride), Cr: chromium, Cys-SAM: cysteamine SAM, scAb: recombinant single-chain antibody

4.0 Conclusion

Prostate cancer is responsible for 29% of all cancer's cases with a record of 13% deaths worldwide. Its 'silent' nature means the symptoms are hardly detectable, therefore when the symptoms prevail, it already signifies the metastasized form of cancer. In response, this paper reports the development work on an Aptasensor-based PSA biosensing assay for early cancer prognosis. The in-house fabricated gold interdigitated triple microelectrodes sensors yield an excellent sensitivity of 2.710 kΩ/$\log_{10}$ ([PSA] ng/ml) and LOD down to 0.38 ng/ml, besides a linear detection ranging from 0.5 ng/ml to 5000 ng/ml, covering the clinical PSA threshold value of 4 ng/ml for occurrence of prostate cancer, and also the crucial 'grey zone' of 4 ng/ml to 10 ng/ml which usually leads to false diagnoses. Furthermore, the limit of detection reported in this paper

is among the lowest for detection of PSA. The sensors exhibited good reproducibility, as evident from the low R.S.D at 4.24% (n=3), hence proving the high sensitivity, great selectivity for detecting PSA with more than 7-fold increase in detection signal versus HSA and more than 6-fold increase versus hK2. The reported assay demonstrates the analytical reliability with an acceptable detection stability of six (6) days for the aptasensor. The principal benefit of the developed sensors is the architecture was designed to allow for greater flexibility of surface functionalization techniques and integration of various nanoparticles or nanostructures to enhance the sensitivity and detection limits.

Acknowledgments

References

Acres, R.G., Ellis, A. V., Alvino, J., Lenahan, C.E., Khodakov, D.A., Metha, G.F., Andersson, G.G., 2012. Molecular structure of 3-Aminopropyltriethoxysilane layers formed on silanol-terminated silicon surfaces. J. Phys. Chem. C 116, 6289–6297. doi:10.1021/jp212056s

Arya, S.K., Bhansali, S., 2012. Anti-prostate specific antigen (Anti-PSA) modified interdigitated microelectrode-based impedimetric biosensor for PSA detection. Biosens. J. 1, 1–7. doi:10.4303/BJ/H110601

Arya, S.K., Zhurauski, P., Jolly, P., Batistuti, M.R., Mulato, M., Estrela, P., 2018. Capacitive aptasensor based on interdigitated electrode for breast cancer detection in undiluted human serum. Biosens. Bioelectron. 102, 106–112. doi:10.1016/j.bios.2017.11.013

Bagheri, E., Abnous, K., Alibolandi, M., Ramezani, M., Taghdisi, S.M., 2018. Triple-helix molecular switch-based aptasensors and DNA sensors. Biosens. Bioelectron. 111, 1–9. doi:10.1016/j.bios.2018.03.070

Cao, X., Pettit, M.E., Conlan, S.L., Wagner, W., Ho, A.D., Clare, A.S., Callow, J.A., Callow, M.E., Grunze, M., Rosenhahn, A., 2009. Resistance of polysaccharide coatings to proteins, hematopoietic cells, and marine organisms. Biomacromolecules 10, 907–915. doi:10.1021/bm8014208

Chung, S., Moon, J.-M., Choi, J., Hwang, H., Shim, Y.-B., 2018. Magnetic force assisted electrochemical sensor for the detection of thrombin with aptamer-antibody sandwich formation. Biosens. Bioelectron. 117, 480–486. doi:10.1016/j.bios.2018.06.068

Dalila R, N., Md Arshad, M.K., Gopinath, S.C.B., Norhaimi, W.M.W., Fathil, M.F.M., 2019. Current and future envision on developing biosensors aided by 2D molybdenum disulfide (MoS2) productions. Biosens. Bioelectron. 132, 248–264. doi:10.1016/j.bios.2019.03.005

Dietrich, P.M., Glamsch, S., Ehlert, C., Lippitz, A., Kulak, N., Unger, W.E.S., 2016. Synchrotron-radiation XPS analysis of ultra-thin silane films: Specifying the organic silicon. Appl. Surf. Sci. 363, 406–411. doi:10.1016/j.apsusc.2015.12.052

Evans, S., 1997. Correction for the effects of adventitious carbon overlayers in quantitative XPS analysis. Surf. Interface Anal. 25, 924–930. doi:10.1002/(SICI)1096-9918(199711)25:12<924::AID-SIA317>3.0.CO;2-2

Feng, C., Dai, S., Wang, L., 2014. Optical aptasensors for quantitative detection of small biomolecules: A review. Biosens. Bioelectron. 59, 64–74. doi:10.1016/j.bios.2014.03.014

Gopinath, S.C.B., 2011. Aptamers, in: Encyclopedia of Analytical Chemistry. John Wiley & Sons, Ltd, Chichester, UK, pp. 1–29. doi:10.1002/9780470027318.a1402.pub2

Hongrong Cai, H., 2018. Therapeutic monoclonal antibodies approved by FDA in 2017. MOJ Immunol 6, 82–84. doi:10.15406/moji.2018.06.00198

Ibau, C., Md Arshad, M.K., Gopinath, S.C.B., 2017. Current advances and future visions on bioelectronic immunosensing for prostate-specific antigen. Biosens. Bioelectron. 98, 267–284. doi:10.1016/j.bios.2017.06.049

Kavosi, B., Salimi, A., Hallaj, R., Moradi, F., 2015. Ultrasensitive electrochemical immunosensor for PSA biomarker detection in prostate cancer cells using gold nanoparticles/PAMAM dendrimer loaded with enzyme linked aptamer as integrated triple signal amplification strategy. Biosens. Bioelectron. 74, 915–923. doi:10.1016/j.bios.2015.07.064

Madianos, L., Tsekenis, G., Skotadis, E., Patsiouras, L., Tsoukalas, D., 2018. A highly sensitive

impedimetric aptasensor for the selective detection of acetamiprid and atrazine based on microwires formed by platinum nanoparticles. Biosens. Bioelectron. 101, 268–274. doi:10.1016/j.bios.2017.10.034

Miodek, A., Regan, E.M., Bhalla, N., Hopkins, N.A.E., Goodchild, S.A., Estrela, P., 2015. Optimisation and characterisation of anti-fouling ternary SAM layers for impedance-based aptasensors. Sensors (Switzerland) 15, 25015–25032. doi:10.3390/s151025015

Park, J., Kim, H., Lee, J.-H., Park, J., Kim, J., Hwang, K., Lee, B., 2018. Amyloid Beta detection by Faradaic electrochemical impedance spectroscopy using interdigitated microelectrodes. Sensors 18, 426. doi:10.3390/s18020426

Savory, N., Abe, K., Sode, K., Ikebukuro, K., 2010. Selection of DNA aptamer against prostate specific antigen using a genetic algorithm and application to sensing. Biosens. Bioelectron. 26, 1386–1391. doi:10.1016/j.bios.2010.07.057

Seok Kim, Y., Ahmad Raston, N.H., Bock Gu, M., 2016. Aptamer-based nanobiosensors. Biosens. Bioelectron. 76, 2–19. doi:10.1016/j.bios.2015.06.040

Shrivastava, A., Gupta, V., 2011. Methods for the determination of limit of detection and limit of quantitation of the analytical methods. Chronicles Young Sci. 2, 21. doi:10.4103/2229-5186.79345

Spain, E., Gilgunn, S., Sharma, S., Adamson, K., Carthy, E., O'Kennedy, R., Forster, R.J., 2016. Detection of prostate specific antigen based on electrocatalytic platinum nanoparticles conjugated to a recombinant scFv antibody. Biosens. Bioelectron. 77, 759–766. doi:10.1016/j.bios.2015.10.058

Stein, C.A., Castanotto, D., 2017. FDA-approved oligonucleotide therapies in 2017. Mol. Ther. 25, 1069–1075. doi:10.1016/j.ymthe.2017.03.023

Tang, Z., Fu, Y., Ma, Z., 2017. Bovine serum albumin as an effective sensitivity enhancer for peptide-based amperometric biosensor for ultrasensitive detection of prostate specific antigen. Biosens. Bioelectron. 94, 394–399. doi:10.1016/j.bios.2017.03.030

Vandenberg, E.T., Bertilsson, L., Liedberg, B., Uvdal, K., Erlandsson, R., Elwing, H., Lundström, I., 1991. Structure of 3-aminopropyl triethoxy silane on silicon oxide. J. Colloid Interface Sci. 147, 103–118. doi:10.1016/0021-9797(91)90139-Y

Wang, C., Qian, J., An, K., Ren, C., Lu, X., Hao, N., Liu, Q., Li, H., Huang, X., Wang, K., 2018. Fabrication of magnetically assembled aptasensing device for label-free determination of aflatoxin B1 based on EIS. Biosens. Bioelectron. 108, 69–75. doi:10.1016/j.bios.2018.02.043

Wang, Y., Qu, Y., Liu, G., Hou, X., Huang, Y., Wu, W., Wu, K., Li, C., 2015. Electrochemical immunoassay for the prostate specific antigen using a reduced graphene oxide functionalized with a high molecular-weight silk peptide. Microchim. Acta 182, 2061–2067. doi:10.1007/s00604-015-1552-2

Zapatero-Rodríguez, J., Liébana, S., Sharma, S., Gilgunn, S., Drago, G.A., O'Kennedy, R., 2018. Detection of free prostate-specific antigen using a novel single-chain antibody (scAb)-based magneto-immunosensor. Bionanoscience 8, 680–689. doi:10.1007/s12668-017-0394-2

Zhu, M., Lerum, M.Z., Chen, W., 2012. How to prepare reproducible, homogeneous, and hydrolytically stable Aminosilane-derived layers on silica. Langmuir 28, 416–423. doi:10.1021/la203638g

Zhurauski, P., Arya, S.K., Jolly, P., Tiede, C., Tomlinson, D.C., Ko Ferrigno, P., Estrela, P., 2018.

Sensitive and selective Affimer-functionalised interdigitated electrode-based capacitive biosensor for Her4 protein tumour biomarker detection. Biosens. Bioelectron. 108, 1–8. doi:10.1016/j.bios.2018.02.041